Computational and Structural Biotechnology Journal 20 (2022) 925–936

COMPUTATIONAL AND STRUCTURAL BIOTECHNOLOGY JOURNAL

journal homepage: www.elsevier.com/locate/csbj

Mechanistic insight into the impact of a bivalent ligand on the structure and dynamics of a GPCR oligomer

Samman Mansoor [a], Gülru Kayık [b], Serdar Durdagi [b], Ozge Sensoy [c,d,*]

[a] School of Engineering and Natural Sciences, Department of Biomedical Engineering and Bioinformatics, Istanbul Medipol University, Istanbul 34810, Turkey
[b] Computational Biology and Molecular Simulations Laboratory, Department of Biophysics, School of Medicine, Bahcesehir University, Istanbul, Turkey
[c] Regenerative and Restorative Medicine Research Center (REMER), Research Institute for Health Sciencesand Technologies (SABITA), Istanbul Medipol University, 34810 Istanbul, Turkey
[d] School of Engineering and Natural Sciences, Department of Computer Engineering, Istanbul Medipol University, Turkey

ARTICLE INFO

Article history:
Received 23 August 2021
Received in revised form 25 December 2021
Accepted 17 January 2022
Available online 4 February 2022

Keywords:
G protein-coupled receptor
Heterobivalent ligand
Accelerated molecular dynamics
Oligomerization

ABSTRACT

Development of effective bivalent ligands has become the focus of intensive research toward modulation of G protein-coupled receptor (GPCR) oligomers, particularly in the field of GPCR pharmacology. Experimental studies have shown that they increased binding affinity and signaling potency compared to their monovalent counterparts, yet underlying molecular mechanism remains elusive. To address this, we performed accelerated molecular dynamics simulations on bivalent-ligand bound Adenosine 2A receptor ($A_{2A}R$) dimer in the context of a modeled tetramer, which consists of $A_{2A}R$ and dopamine 2 receptor (D_2R) homodimers and their cognate G proteins. Our results demonstrate that bivalent ligand impacted interactions between pharmacophore groups and ligand binding residues, thus modulating allosteric communication network and water channel formed within the receptor. Moreover, it also strengthens contacts between receptor and G protein, by modulating the volume of ligand binding pocket and intracellular domain of the receptor. Importantly, we showed that impact evoked by the bivalent ligand on $A_{2A}R$ dimer was also transmitted to *apo* D_2R, which is part of the neighboring D_2R dimer. To the best of our knowledge, this is the first study that provides a mechanistic insight into the impact of a bivalent ligand on dynamics of a GPCR oligomer. Consequently, this will pave the way for development of effective ligands for modulation of GPCR oligomers and hence treatment of crucial diseases such as Parkinson's disease and cancer.

1. Introduction

G protein-coupled receptors (GPCRs) mediate most of our physiological responses to stimulants by coherent action of various modulators such as orthosteric/allosteric ligands, membrane and receptor partners, collective interaction of which leads to formation of GPCR oligomers. In these supramolecular structures, continuous information flow among the protomers transforms GPCR homo/heteromers into allosteric hubs, thus altering functional behavior of individual receptors. Over the last decades, it has been thought that the supramolecular structure, which is composed of a GPCR homodimer and G protein, constitutes the main functional unit of GPCR signalosomes [1–4]. Indeed, a recent experimental study has shown that a GPCR heterotetramer is comprised of homodimers of $A_{2A}R$ and D_2R along with their cognate G proteins [5].

GPCRs are involved in pathologies of many crucial diseases such as Parkinson's disease (PD), Alzheimer's disease (AD), diabetes, and cancer, thus making them hot targets in drug discovery studies [6–9]. On the other hand, allosteric interactions present in GPCR oligomers make targeting this class of proteins challenging in the field of GPCR pharmacology [10]. As a notable example, PD can be considered, which is caused by the loss of neurons that produce dopamine in substantia nigra [11]. As an effective therapy, dopaminergic agonists have been considered to increase dopamine level but remained insufficient [12–14]. It was after the discovery of antagonistic impact of $A_{2A}R$ on D_2R, where $A_{2A}R$ decreases affinity and intrinsic efficacy of dopamine at D_2R protomer [15], $A_{2A}R$

* Corresponding author at: Regenerative and Restorative Medicine Research Center (REMER), Research Institute for Health Sciencesand Technologies (SABITA), Istanbul Medipol University, 34810 Istanbul, Turkey.
E-mail addresses: sammanmansoor9@gmail.com (S. Mansoor), gulru.kayik@gmail.com (G. Kayık), serdardurdagi@gmail.com (S. Durdagi), osensoy@medipol.edu.tr (O. Sensoy).

https://doi.org/10.1016/j.csbj.2022.01.016
2001-0370/

antagonists have been used as combination therapy along with D_2R agonists in treatment of PD [16]. Recently, it has been shown that $A_{2A}R$-D_2R assemble into a tetrameric structure which is composed of a pair of this dimer. Moreover, it has been also demonstrated that simultaneous occupation of both $A_{2A}R$ protomers by an agonist and an antagonist in the tetramer does not induce an allosteric modulation of D_2R agonist binding and intrinsic efficacy [5]. Therefore, this suggests that effective modulation of GPCR oligomers requires simultaneous targeting of individual receptors. Also, this shows that simultaneous occupation of one of the dimers in the tetramer impacts the function of the other dimer as well. Hence, bivalent ligands have emerged as useful tools to simultaneously target receptor dimers within the oligomer [17,18]. A bivalent ligand is composed of two pharmachopores, which are covalently linked by a spacer group and can be categorized into two groups: homo- and heterobivalent ligands which consist of same and different pharmacophore groups, respectively. There has been a couple of experimental studies where the optimum length of the spacer and stability of the bivalent ligand were determined using computational tools, and their biological activities were also tested by *in vitro* studies [19,20]. However, none of them provide a mechanistic insight into the impact of these special class of ligands on structure and dynamics of receptors which is crucial for development of effective ligands with precise targeting capabilities.

In this study, we investigated impact of a designed bivalent ligand on dynamics of $A_{2A}R$ dimer in the context of a tetramer, which has been shown to form the signaling unit pertaining to $A_{2A}R$-D_2R oligomer [5] using accelerated molecular dynamics simulations. To do so, we performed simulations on the tetramer model in the presence and absence of the linker (including only pharmacophore groups, but not the spacer and biphenyltriazole moiety) [21–23]. We investigated how i) conformational preferences of key residues that are involved in receptor activation, ii) allosteric interaction network, iii) membrane interactions of the receptors, iv) water channel formation, and v) coupling with effector G protein are modulated by the bivalent ligand. This study provides a mechanistic insight into the impact of a bivalent ligand on dynamics of the GPCR oligomer, thus assigning additional roles to linkers as modulators of GPCR oligomers.

2. Materials and methods

2.1. Tetramer modeling

The crystal structure of the tetramer is not available but interaction interfaces in homo- and heterodimers were revealed in a recent experimental study [22]. According to that, i) homodimer and heterodimer interfaces were built up of TM6 and TM4/TM5, respectively, and ii) agonist-bound protomers complex with effectors were located at the periphery of the tetramer to accommodate G proteins. Before modeling the dimers, first receptor monomers were modeled. In particular, CGS-21680-bound $A_{2A}R$ mini $G\alpha_s$ complex, we have used crystal structures of NECA-bound $A_{2A}R$ mini $G\alpha_s$ complex (with RAS-like domain)(PDB ID:55G53) [24] as a template since NECA shares similar chemical groups with CGS-21680. In fact, the crystal structure of CGS-21680-bound A_{2A} (PDB ID:44UHR) [16] is available but it cannot accommodate G protein because of the narrower opening of the intracellular site of the receptor. Therefore, we aligned the two structures and observed that residues that interact with the ligand were aligned well. Consequently, CGS-21680 was transferred from 4UHR to 5G53. For modeling istradefylline-bound $A_{2A}R$, we used crystal structure of $A_{2A}R$ bound with ZM241385 (PDB ID:44EIY) [25] since it shares similar chemical structure with the target ligand. The Na^+ ion which is present in allosteric site of antogonist bound $A_{2A}R$ was kept in our construct from the original crystal structure of 4EIY. We performed induced fit docking, which is implemented in Schrodinger's Glide docking software [26,27] to find best possible pose for istradefylline within the binding pocket using the hydrogen bond as a restraint with $ASN253^{6.55}$ (superscripts denote Ballesteros-Weinstein numbering) [28] residue of the receptor.

As to the D_2R dimer, we used crystal structure of D_2R bound with risperodine (PDB ID:66CM4) [29] for modeling *apo* D_2R by removing T4 lysozyme which is fused to ICL3 of the receptor. The crystal structure of μ-opioid receptor complex with mini $G\alpha_i$ (PDB ID:6DDF) [30] was used for modeling quinpirole-bound D_2R-$G\alpha_i$ complex since the crystal structure of D_2R-G_i complex was not available at the time of simulations were done. The sequence similarity between μ-opioid and D_2R was 35%. After it's release, we also compared backbone root mean square deviation (RMSD) between 6DDF and 6VMS (D_2R complex with G_i) and found to be 1Å. To find the best possible pose of the ligand we performed induced fit docking by using the hydrogen bond as a restraint with $ASP114^{3.32}$ residue of the receptor. Herein, it is important to emphasize that D_2R has a long ICL3 which is not resolved in crystal structures. We modeled the missing regions as a loop by using the first 60 amino acids of ICL3 to prevent any restraint that may be introduced upon smaller length of loops.

For modeling dimers, we downloaded all the available crystal structures of GPCRs from G protein-coupled receptors database (GPCRdb) (245 structures were present as of April, 2018) to use as templates for generating corresponding homo- and heterodimer interfaces in the tetramer. First, the crystal mates were generated in Maestro, and then, receptor monomers were aligned to corresponding monomers of the templates. In particular, we could get 38 templates with TM4/TM5 and 2 templates with TM6/TM6 dimerization interfaces, the list of which can be found in the Supplementary Table. In fact, various different orientations of the monomers in the dimer can satisfy those interfaces but we made use of the experimental data [22] to further pick up the biologically relevant interfaces. Accordingly, the crystal structures with PDB IDs:5WIU [30] and 5O9H [31] were used to model TM6/TM6 and TM4/TM5 interfaces, respectively. Slight steric clashes in the models were alleviated by using Prime module of Maestro program.

2.2. System preparation

Protein structure preparation was performed using "Protein Preparation Wizard" implemented in Maestro molecular modeling package [32]. Non-protein entities like BRIL, which is included in the crystal structure of ZM241385-bound $A_{2A}R$ (PDB ID:44EIY), was removed and the missing region was filled by original residues of the receptor using "Cross-Link Protein" module implemented under Bioluminate [33] panel of Schrondinger software. Also, missing regions present either in receptors or in mini G proteins were filled similarly. Missing hydrogen atoms were added using PROPKA [34] to maintain protonation state of residues at pH:7.0. H-atoms were optimized and constrained energy minimization was carried out on the final tetramer model was obtained. The tetramer was aligned in the membrane using Orientations of Proteins in Membrane (OPM) server [35,36] and then prepared using Membrane Bilayer builder program [37] implemented in CHARMM-GUI server [38]. The membrane was prepared to include 30% cholesterol and 70% sphingomyelin molecules to mimic lipid rafts, thus resulting with a total number of *ca* 500000 atoms. TIP3P [39] and CHARMM36m force fields [40] were used to model water molecules and protein in the system. Ligand parametrization was done using CGenFF, implemented in CHARMM-GUI server [41]. The output files were examined to check if penalty values associated with ligands exceeded the threshold level but they didn't exceed.

2.3. Bivalent ligand construction

The bivalent ligand was modeled to consist of two pharmacophore groups, namely, istradefylline and CGS-21680 along with the linker, in accordance with the experimental data [5]. The linker, which was shown to bind to a heterodimer [21], was composed of an affinity-generating biphenyltriazole-moiety along with a spacer group. After modeling the tetramer, it was examined to determine possible regions on the pharmacophore groups to which the linker was attached. Consequently, methoxy groups of istradefylline and carboxyl group of CGS-21680 were found to be accessible from the extracellular domain of the receptors and the linker was added to these regions using "build" panel of Schrodinger software. The final chemical composition of the linker was determined by considering possible synthesis opportunities of the bivalent ligand. In addition, to determine the optimum length of the linker we performed MD simulations on the structures having different linker lengths for 250 ns. Analysis of these trajectories showed that linker lengths that were shorter than 48Å were unstable and left the ligand binding pocket during the simulation (See SI Movie). Importantly, as the length was further increased, the RMSD of the linker tended to decrease until the length of 52Å. After that value, we did not observe any further decrease in the RMSD, hence used that linker in our further simulations [21] (See Fig. 1).

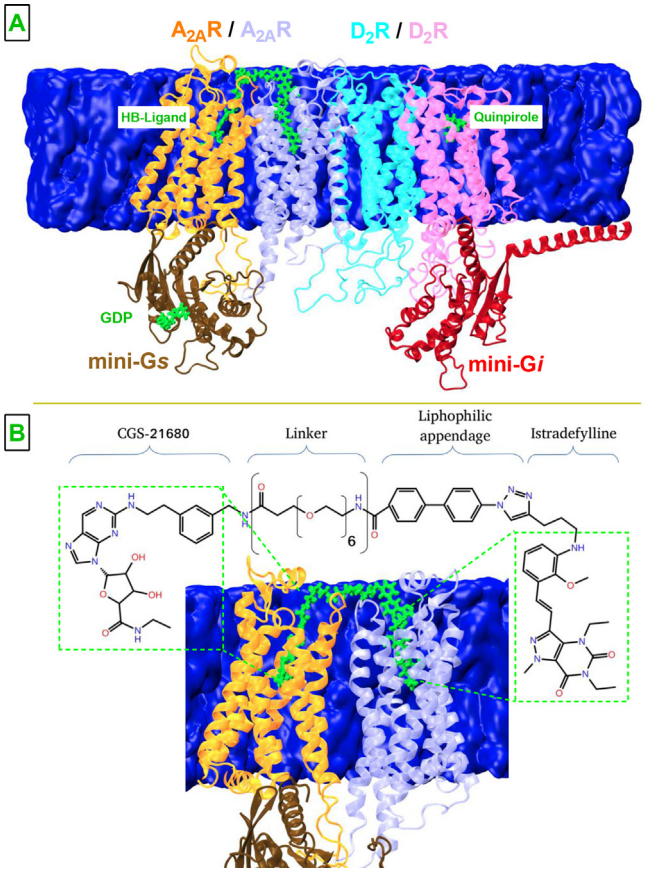

Fig. 1. $A_{2A}R/D_2R$ tetramer with bivalent ligand A. Schematic representation of the system used in this study. The membrane is shown in blue. $A_{2A}R$ protomers and mini-Gα_s are shown in orange, purple and brown, respectively and new cartoon representation whereas bivalent ligand is shown in green and licorice representation. Water molecules are omitted for the sake of simplicity. D_2R protomers and mini-Gα_i are shown in pink, cyan, and red, respectively. **B**. Representation of the chemical structure of the linker. The pharmacophore groups and the linker are shown in detail together with $A_{2A}R$ dimer.

2.4. Molecular dynamics simulation

In this study, we performed both classical (cMD) and accelerated molecular dynamics (aMD) simulations using Nanoscale Molecular dynamics NAMD [42] package. For aMD, "dual-boost" was chosen to enhance sampling of the conformational space and performed by getting average potential energy values from cMD simulations. Specifically, the systems studied were heated from 0 K to 310 K within 1 ns and pre-equilibrated using NVT ensemble at 310 K for 50 ns. This was followed by 500 ns cMD simulations which were performed using NPT ensemble at 1 atm and 310 K to get average potential energies, from which the acceleration parameters were calculated. The last snapshots of these simulations were used as starting conformations in aMD simulations and aMD simulations were performed for 1μs. Nose–Hoover [43] and Parrinello-Rahman [44] coupling algorithms were used to maintain constant temperature and pressure, respectively throughout simulations. The integration step of 2*fs* was used in all simulations performed. In the dual-boost aMD, a dihedral potential and a potential boost were added to all the atoms in the systems. The dihedral and potential boost acceleration parameters were calculated using following equations:

$$E_{dihed} = V_{dihed-avg} + \lambda * V_{dihed-avg}, \quad (1)$$

$$\alpha_{dihed} = \lambda * V_{dihed-avg}/5 \quad (2)$$

$$E_{total} = V_{total-avg} + 0.2 * N_{atoms}, \quad (3)$$

$$\alpha_{total} = 0.2 * N_{atoms}, \quad (4)$$

where N_{atoms} is the total number of atoms, and $V_{dihed-avg}$ and $V_{total-avg}$ are the average dihedral and potential energies obtained from cMD simulations. λ is an adjustable acceleration parameter. We used 0.3 for λ which was shown to perform effectively for GPCR systems [45]. The systems were simulated twice, each of which was simulated starting with a different initial velocity distribution. The reweighted PMF profiles were obtained using cumulant expansion to the 2nd order; however, reweighting caused a large energetic noise because of large system size of the system as shown in SI Fig. 1. Considering that the overall shape of free energy profiles is maintained in aMD simulations, unweighted data should provide an estimate of the free energy differences [46,47]. Therefore, unweighted free energy profiles are presented in this study (See SI Fig. 1 and 2 for detailed discussion [48,49]).

2.5. Cross-correlation analysis

To calculate the extent of correlation among residues, dynamic cross-correlation maps were obtained. According to that, normalized co-variance values of residues were computed by considering Cα atoms [50] and using the following equation:

$$DCC(i,j) = \frac{< \Delta r_i(t).\Delta r_j(t) >_t}{\sqrt{< \|\Delta r_i(t)\|^2 >_t}\sqrt{< \|\Delta r_j(t)\|^2 >_t}} \quad (5)$$

where $r_i(t)$ and $r_j(t)$ represents the coordinates of the i^{th} and j^{th} atoms as a function of time t, $<>$ indicates the time ensemble average, $\Delta r_i(t) = r_i(t) - (< r_i(t) >)_t$ and $\Delta r_j(t) = r_j(t) - (< r_j(t) >)_t$. The correlation range of residues lies within -1.0 to 1.0, where positive correlated displacement falls between $(0 - 1.0)$ whereas anti-correlation displacement falls between $(-1.0 - 0)$.

2.6. Network construction

Network analysis was carried out using PSN-Ensemble Software [51] by considering side chain atoms of the residues in $A_{2A}R$ receptor. As an input, two residues were provided as the source and the sink Glu169$^{4.90}$ and Ile292$^{7.57}$, which were distant from each other

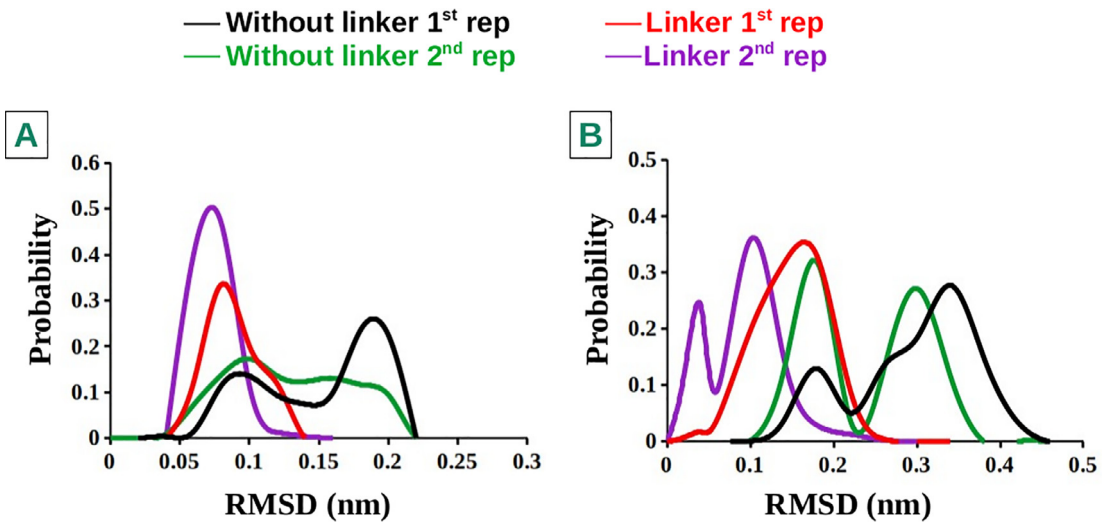

Fig. 2. Root Mean Square Deviation (RMSD) timeline plots. A. Antagonist bound $A_{2A}R$. **B.** Agonist bound $A_{2A}R$.

on the protein and between which allosteric communication signal was generated. Herein, cross correlation matrices were used as inputs to calculate and weigh the shortest communication pathways used by the receptor in the presence and absence of the bivalent ligand.

2.7. Binding volume calculation

Ligand binding and G protein binding volumes were calculated using KvFinder plugin of pymol, which is based on geometrical grid-based method combined with space segmentation capabilities [52]. The space defined between molecular surfaces of the two probes is known as the cavity. The probe-in was set to 0.8Å and probe-out was set to 8.0Å with volume of cavity as 200ÅFor ligand binding pocket Ile16$^{1.42}$, Ala59$^{2.57}$, Thr68$^{2.66}$, His75$^{3.23}$, Val86$^{3.34}$, Phe183$^{5.44}$, Trp246$^{6.48}$, Phe258$^{6.60}$ and His278$^{7.43}$ were selected and Ser35$^{1.61}$, Gln38$^{1.64}$, Pro109$^{3.57}$, Ile200$^{5.61}$, Ala204$^{5.65}$, Gln226$^{6.27}$ and Arg293$^{7.58}$ residues were selected for calculating the volume of G-protein binding pocket.

3. Results

3.1. Optimum linker length is required for stable binding of bivalent ligand to $A_{2A}R$ dimer

As explained in the Methods section tetramer was modeled to consist of dimers of $A_{2A}R$ and D_2R along with their corresponding effectors, mini-Gα_s and mini-Gα_i, respectively, to be in line with experimental data [5]. In a follow-up study of Navarro *et.al* [22], homodimer interfaces were shown to consist of TM6 whereas heterodimer interface was shown to consist of TM4/TM5. According to the same study, it was also suggested that protomers which were bound to G protein should be located on the periphery of the quaternary structure to prevent clashes between two G proteins whereas *apo* D_2R and antagonist-bound $A_{2A}R$ were found in the middle. To identify possible attachment points of pharmacophores with the linker, crystal structures of CGS-21680 (PDB ID4UHR) [16] and ZM241385-bound $A_{2A}R$ (PDB ID4EIY) [25] were used. Examination of these structures revealed that methoxy groups of istradefylline and carboxyl group of CGS-21680 were accessible from the extracellular domain of the receptors. Therefore, these two points were linked to each other using an affinity generating biphenyltriazole-moiety and spacer as shown in Fig. 1. Since biphenyltriazole-moiety acts as an affinity-generating group it is anticipated that inclusion of this group in the linker might shorten the time required to observe any possible impact of the linker on the dynamics of the system [60,61]. To determine the optimum linker length we performed classical molecular dynamics (cMD) simulations with bivalent ligands having different number of spacer units. In fact, we measured the minimum distance (beeline) between the two attachment points of the linker as 45 Å. However, our results showed that bivalent ligand which was shorter than 48Åcould not stably bind to the dimer (See Supplementary Movie) which was in correspondence with a study of Hubner et.al [21]. The reason why the linkers with distance shorter than 48Åcould not stably bind was that they clashed with extracellular loops of the protomers, which were protruded from the receptors. It is also important to emphasize that the linker stabilizes pharmacophores compared to their monovalent counterparts as revealed by smaller RMSD values measured in the presence of the linker (See Fig. 2).

3.2. Extra- and intracellular domains are stabilized and global dynamics is restricted by the linker in $A_{2A}R$ dimer

The bivalent ligand was built to composed of an $A_{2A}R$ antagonist (istradefylline) and an agonist (CGS-21680), where affinity-generating biphenyltriazole moiety was connected to istradefylline. Comparative analyses of the trajectories showed that the linker made contacts with extracellular loop (ECL) 1 and 3, thus decreasing fluctuation at these regions in antagonist-bound $A_{2A}R$ as shown in Fig. 3. Specifically, side chains of Thr68$^{2.56}$ and Asp261$^{6.63}$/Ser263$^{6.65}$, which are located on ECL1 and ECL3, respectively made hydrogen bonds with nitrogen atoms located on the linker. Moreover, the linker also decreased conformational fluctuation at intracellular loop (ICL) 2, TM1, TM6 and TM7, last two of which were included at homodimer interface. On the other hand the linker did not impact fluctuations in agonist-bound $A_{2A}R$/mini-Gα_s complex. Here, it is important to emphasize that the impact of the linker on agonist-bound $A_{2A}R$/mini-Gα_s was reflected in the number of contacts made between the ligand and certain residues of ligand binding pocket of receptor. It was increased by ~50% in agonist-bound $A_{2A}R$/mini-Gα_s while remained the same in antagonist-bound receptor. Specifically, contacts between Trp246$^{6.48}$ and Ile274$^{7.39}$, which have been implicated in agonist binding, and CGS-21680 increased in the presence of the linker. Having observed that the linker modulated fluctuation pattern of

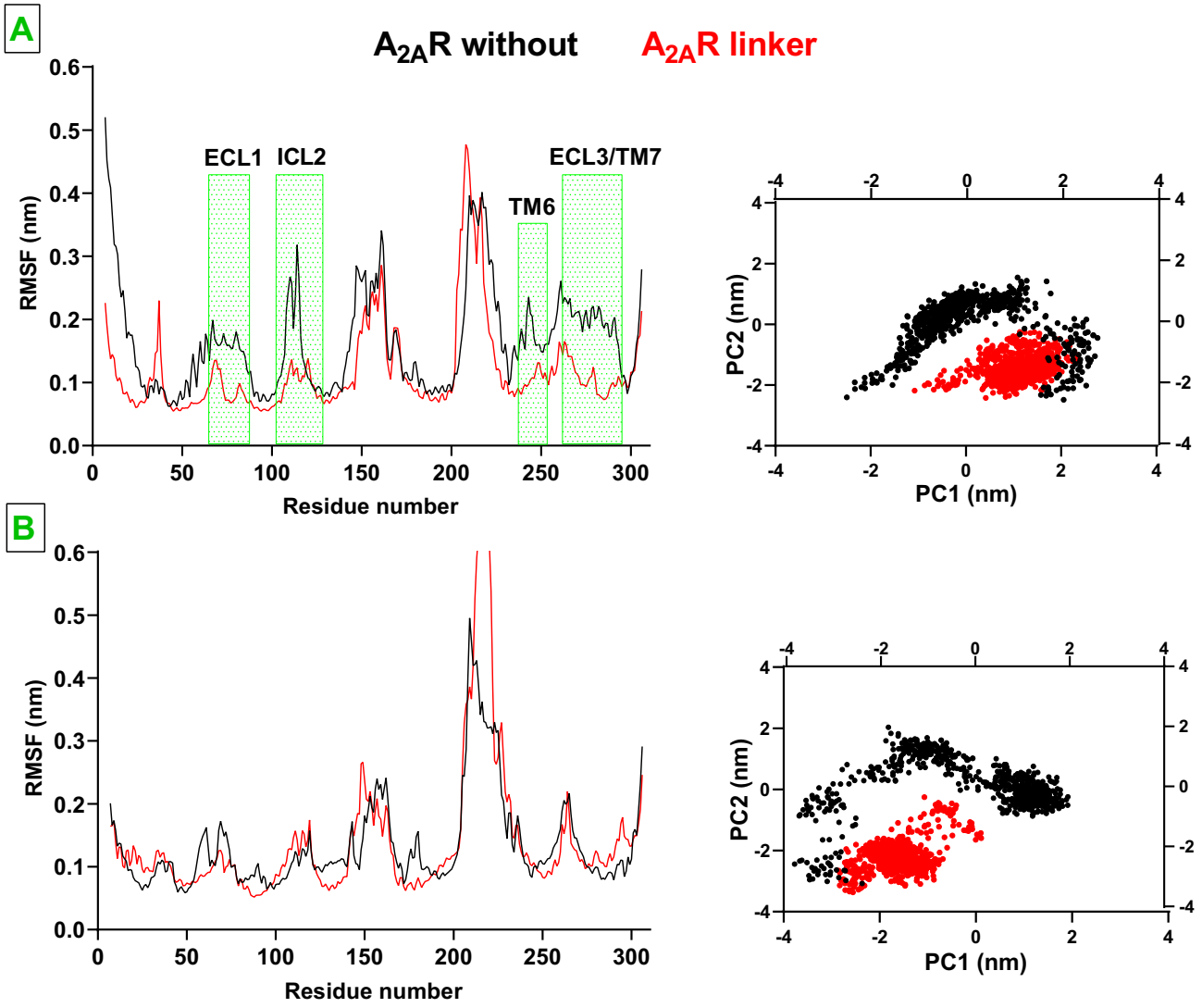

Fig. 3. Root mean square fluctuation (RMSF) and 2D principal component analysis (PCA) profiles pertaining to A. antagonist-bound $A_{2A}R$ and **B**. agonist-bound $A_{2A}R$/mini-Gα_s. The regions that showed difference between without and with linker systems are indicated with green rectangles. The RMSF and 2D-(PCA) plots pertaining to 2nd replicate are given in SI Fig. 4.

residues (See Fig. 3B) we also set out to investigate its impact on the global dynamics of $A_{2A}R$ protomers. Results showed that global motion of the receptors was confined in the presence of the ligand as they sampled narrower region on the conformational space, which was revealed by the first and the second eigenvectors of the systems (See Fig. 3).

3.3. The linker modulates volume of ligand binding pocket and intracellular domain in $A_{2A}R$ dimer

We set out to investigate possible impact of the linker on structure of ligand binding pocket as the number of contacts made between CGS-21680 and receptor increased in the presence of the linker. Interestingly, we observed that volume of the ligand binding pocket was decreased by $\sim$ 15% in CGS-21680- bound $A_{2A}R$ while this change was not significant for istradefylline-bound $A_{2A}R$ protomer (See Fig. 4A). Moreover, we also measured the volume of the G protein binding site of $A_{2A}R$ protomers to investigate if the change observed in the ligand binding pocket was transmitted to the intracellular domain of the receptors. Indeed, the volume of intracellular domain was increased by $\sim$ 10% in CGS-21680-bound $A_{2A}R$/mini-Gα_s (See Fig. 4B). With that, agonist-bound $A_{2A}R$ could achieve such volume range, which was shown to be sampled by active receptors, [53] in the presence of the linker. On the other hand, the volume of the intracellular domain in the absence of the linker was closer to the value which was sampled by the receptor found in an intermediate state between the inactive and active receptor [53]. This change was also reflected in the ionic lock distances as well such that longer distance was observed in agonist-bound $A_{2A}R$ in the presence of the linker, thus having wider intracellular domain. Here, it is important to emphasize that the volume of G protein binding site in istradefylline-bound $A_{2A}R$ decreased despite the absence of a significant change in the volume of ligand binding pocket (See Fig. 4A and 4B). Since istradefylline-bound $A_{2A}R$ was placed between CGS-21680- bound $A_{2A}R$/mini-Gα_s and *apo* D_2R in the tetramer (See Methods for detailed information), expansion of the intracellular domain of neighboring $A_{2A}R$ might confine the space available for antagonist-bound $A_{2A}R$ protomer. Here in, we need to elaborate that expansion of intracellular domain of agonist-bound $A_{2A}R$ also impacted interactions between the receptor and mini-Gα_s: Coulomb energy decreased (became more favorable)

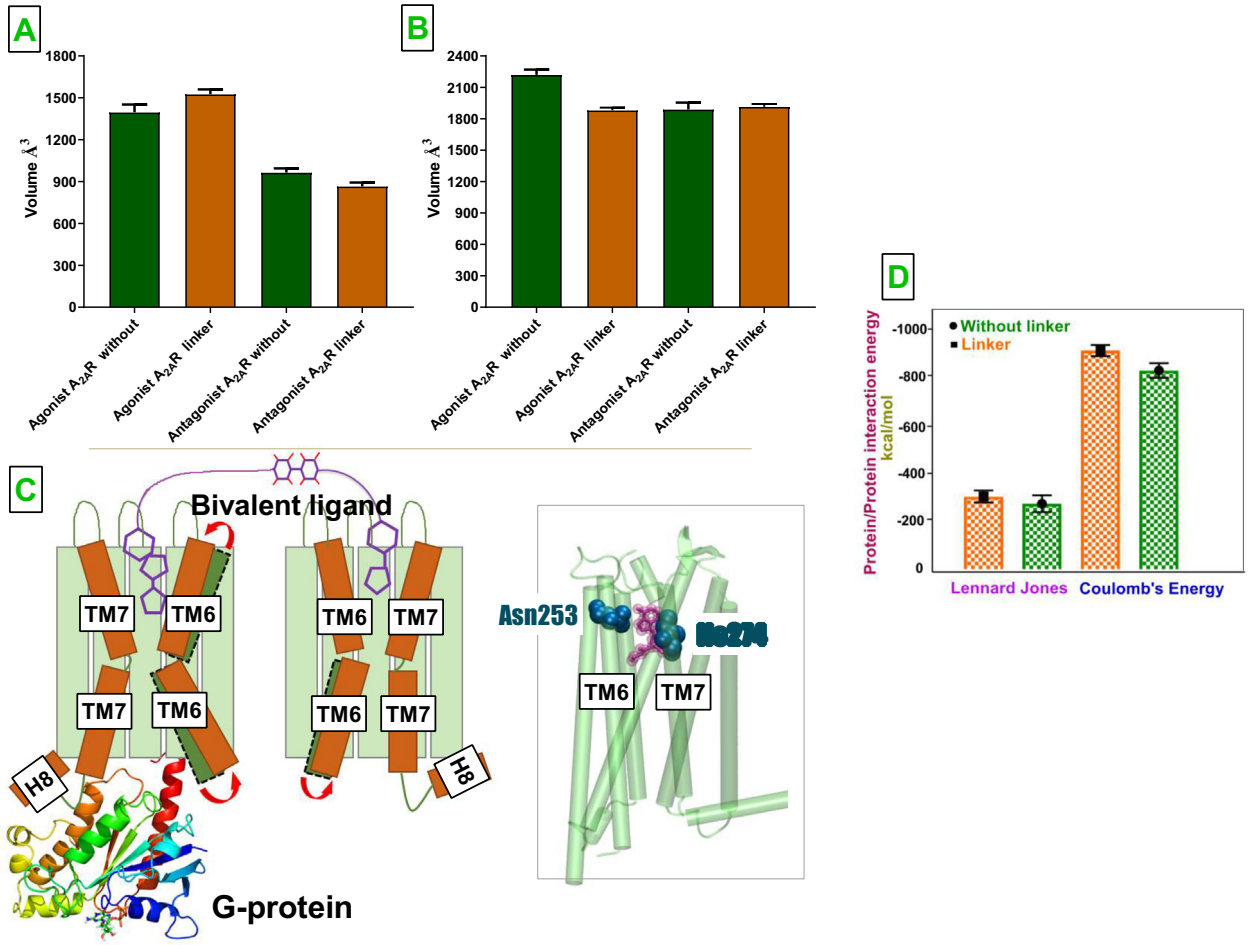

Fig. 4. Changes in volumes of A. ligand binding pocket and **B**. G protein binding domain between without and linker systems **C**. Schematic representation of conformational changes adapted by $A_{2A}R$ receptors in the presence of the linker. The position of transmembrane (TM) 6 and 7 in the absence and presence of the bivalent ligands is shown in green and orange, respectively. Mini-Gα_s that is bound to agonist-bound $A_{2A}R$ is shown in new cartoon representation. Right hand side Ile274$^{7.39}$ interaction with ligand emerge upon adding the linker. **D**. Protein–protein interaction energies measured between G protein and the receptors are also given.

by 10% in the presence of the linker, whereas the change in Lennard Jones energy was not significant between without and linker systems.

3.4. Conformational preferences of microswitches and residue correlations are modulated by the linker in $A_{2A}R$ dimer

Reciprocal changes observed in the volumes of both ligand binding pocket and G protein binding site of CGS-21680-bound $A_{2A}R$ in the presence of the linker suggested alterations in correlation of interactions at certain TM domains. To corroborate such impact, we calculated dynamics cross correlation matrices for the systems studied (See Fig. 5) and showed that strength of correlated motion between TM1 and TM3, TM1 and TM7, TM5 and TM6 as well as TM6 and TM7 was increased in the presence of the linker. However, the strength of anti-correlated motion was increased at TM3/TM6, all of which were occurred upon receptor activation. That is to say, increment in strength of anti-correlated and correlated motion in TM3/TM6 and TM5/TM6 pairs, respectively, triggered wider opening of the intracellular domain of the receptor, which was also reflected in the volume of G protein binding site at CGS-21680-bound $A_{2A}R$. This observation was also in line with a recent study where shrinking of the volume of orthosteric ligand binding site and expansion of the intracellular domain of the receptor were shown to be associated with similar changes occurring in TM3, TM6 and TM7 [54].

Moreover, these rearrangements also led to stabilization of side chains of certain residues at istradefylline-bound $A_{2A}R$ in the presence of the linker. Importantly, Trp246$^{6.48}$ adopted χ_2 angle values which provided close packing of the residue against the sodium ion as seen in the crystal structure of inactive $A_{2A}R$ (PDB ID:4EIY). Also, hydroxyl group of Tyr288$^{7.53}$, which is involved in G protein binding, is positioned farther from the G protein binding site (See Fig. 6) than in without linker system and crystal structure of inactive $A_{2A}R$ (PDB ID:4UHR) [55].

Besides residue correlations, the bivalent ligand also impacted allosteric interaction network in agonist-bound protomer in $A_{2A}R$ dimer. Specifically, TM5 emerged as one of the most significant domain that participated in the interaction network in the presence of the linker. Recalling coupling between orthosteric ligand binding pocket and intracellular domain in agonist-bound $A_{2A}R$, it can be said that the result was in correspondence with a study where allosteric coupling between extra- and intracellular domain of the receptor was shown to be mediated through TM5 [56]. Moreover, Asn253$^{6.55}$ residue, which is one of the key residues of the ligand binding pocket that anchors the exocyclic amine of the ligand's central core, participated to allosteric interaction network in the presence of the linker and interestingly, TM3 didn't contribute in the presence of the linker (See Fig. 7). We also investi-

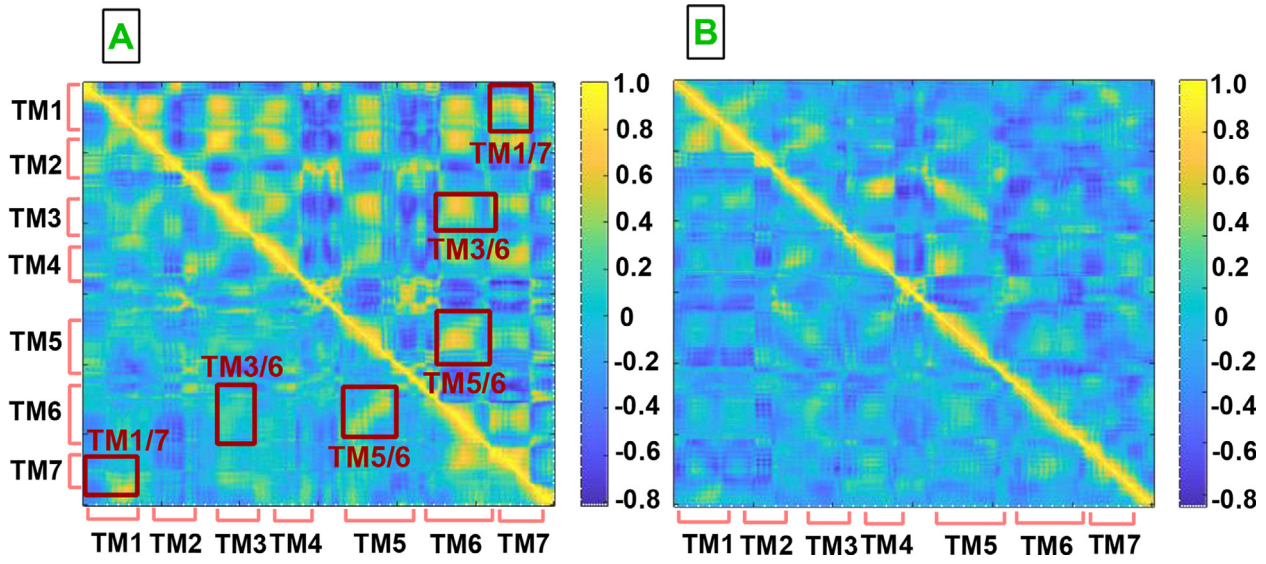

Fig. 5. Dynamic cross correlation maps (DCCM) A. agonist-bound $A_{2A}R$/mini-Gα_s and **B**. antagonist-bound $A_{2A}R$. The upper triangles in A and B correspond to DCCM of the system with linker whereas the lower triangles correspond to those without linker. The DCCM plots are obtained by combining both replicas, and the DCCM plots of each replica is given in SI Fig. 7.

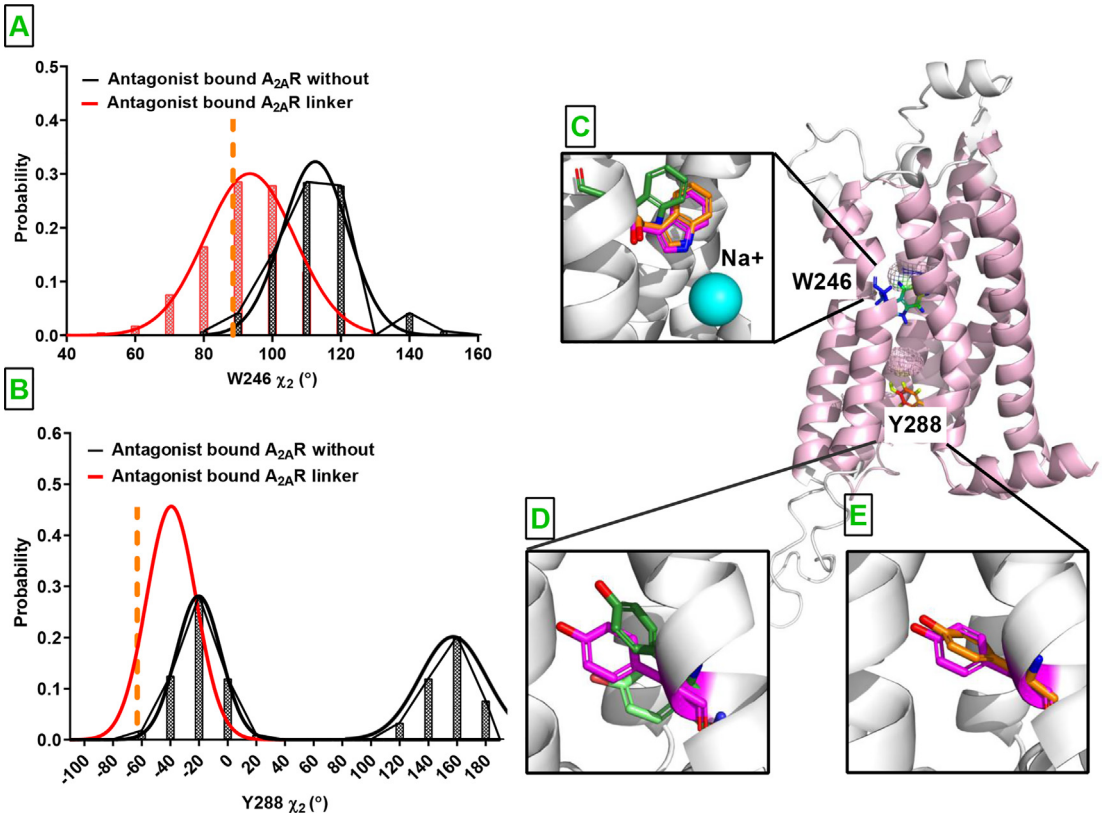

Fig. 6. Angle probability distribution of Trp246 and Tyr288. A. χ_2 of $Trp246^{6.48}$ is presented for antagonist-bound $A_{2A}R$ in the absence and presence of the linker, in black and red, respectively. The corresponding angle is also measured in crystal structure of antagonist-bound $A_{2A}R$ (PDB ID:44EIY) and indicated with dashed orange line. **B**. The same as in A but for χ_2 of $Tyr288^{7.53}$. Comparison of orientation of **C**. $Trp246^{6.48}$ in the absence (green) and presence (orange) of the bivalent ligand. Oreintations of $Tyr288^{7.53}$ in the **D** absence of linker (dark and light green) and **E**. presence of linker (orange). The orientation of $Trp^{6.48}$ and $Tyr^{7.53}$ in the crystal structure of antagonist-bound receptor is shown in pink. The residues are shown on the 3D structure of antagonist bound $A_{2A}R$. Timeline plots of $Trp246^{6.48}$ and $Tyr288^{7.53}$ of both replicates are given in the SI Fig. 6.

gated interactions between $A_{2A}R$ dimer and membrane and showed that $Trp129^{4.50}$, which was shown to be part of the cholesterol consensus motif, of agonist-bound $A_{2A}R$ made close contacts with a cholesterol molecule in the presence of the linker in one of the replicates [57] (See SI Fig. 9). Therein, the cholesterol moved by almost 5Å throughout the trajectory from its original position

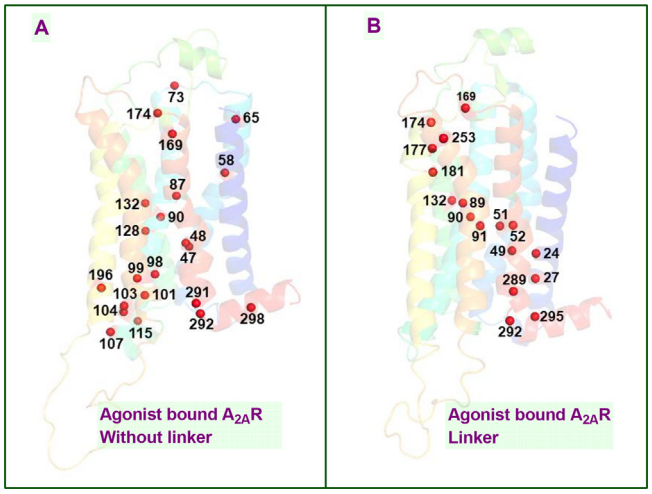

Fig. 7. $A_{2A}R$ Network Pathway.

and eventually contacted to the receptor, whereas no such interaction was observed for the antagonist-bound $A_{2A}R$ neither in the presence nor the absence of the linker. Lastly, we also compared pattern of water channels formed within the receptors between without and linker systems using the VolMap plugin of VMD. In accordance with a study which showed a correlation between receptor activation and continuous water channel formation [53], we observed a continuous water channel in agonist-bound $A_{2A}R$ whereas it was disrupted in antagonist-bound $A_{2A}R$ (See Fig. 8). Interestingly, continuous water channel could be also maintained in the presence of the linker in agonist-bound receptor; however, water density was decreased in the region between the extracellular domain and orthosteric ligand binding pocket as observed in antagonist-bound $A_{2A}R$. Analysis of the trajectories showed that the linker precluded water flow from extracellular side to the inside of the receptor. Consequently, water molecules could be clustered only around Na^+ ion in antagonist-bound receptor.

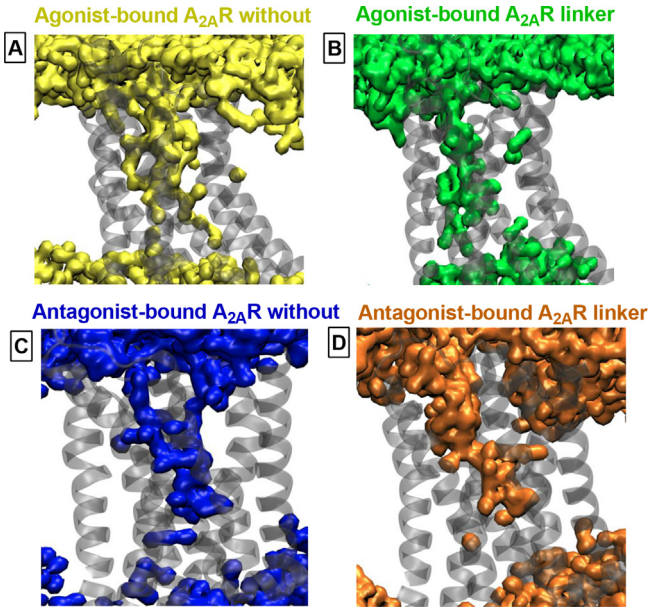

Fig. 8. Internal Water Channel formation. A. Agonist-bound $A_{2A}R$, and **B**. Antagonist-bound $A_{2A}R$ in the absence of the linker, **C**. Agonist-bound $A_{2A}R$, and **D**. Antagonist-bound $A_{2A}R$ in the presence of the linker. Water occupancy maps are computed using the VolMap tool of VMD.

3.5. The linker impacts the dynamics of apo D_2R in the neighboring D_2R dimer

The tetramer is composed of pairs of $A_{2A}R$ and D_2R, where the homodimer interfaces are formed by TM6 and the heterodimer interface is formed by TM4 and TM5. In accordance with experimental data, one of the D_2R protomers was modeled as *apo* and the other protomer was modeled to bound with D_2R agonist, quinpirole and mini-$G\alpha_i$ (See Methods for more details). The results showed that ICL2, albeit to a lesser extent, and ICL3 were stabilized in *apo* D_2R in the presence of the linker while only a small part of the ICL3 could be stabilized in agonist-bound D_2R/mini-$G\alpha_i$(See Fig. 9). Moreover, similar to $A_{2A}R$ dimer, the linker also confined global dynamics of the protomers as revealed by principal component analysis as shown in Fig. 9. Interestingly, the linker also modulated residue correlations at *apo* D_2R despite not being directly bound to the receptor. Specifically, an increase was observed in the strength of correlated motion in residues located on TM3 and TM4, two of which construct the heterodimer interface with antagonist-bound $A_{2A}R$. Moreover, an increase was also observed in the correlated motion of TM3 and TM6 as well as TM3 and TM4 in the presence of the linker in *apo* D_2R indicating that they tend to get closer to each other as shown in (Fig. 10B).

Herein, it is also important to emphasize that the intracellular domain of *apo* D_2R was modulated by the linker as the receptor could sample a wider range of ionic lock distances which are calculated between $Arg132^{3.50}$ ($C\gamma$) and $Glu368^{6.30}$ ($C\delta$) atoms [58] in the absence of the linker whereas it could only sample shorter distances in the presence of the linker.

4. Discussion

Bivalent ligands have long been thought to act solely as connectors of the two pharmacophore groups. On the other hand, experimental studies have shown that binding affinity and signaling potency are increased by bivalent ligands compared to their monovalent counterparts. Consequently, this suggests that these ligands are capable of modulating dynamics of GPCR oligomers; however, underlying mechanism has remained elusive. In this study, to the best of our knowledge, for the first time, we provided a molecular level understanding to dynamics and functional changes induced by the bivalent ligand. In particular, we demonstrated that the linker made interactions with residues located at the extracellular domains of $A_{2A}R$ protomers. Notably, this has led to stabilization of antagonist-bound $A_{2A}R$ while that impact was not remarkable for agonist-bound $A_{2A}R$/mini-$G\alpha_s$ as revealed by root-mean-square fluctuation patterns. Interestingly; however, this caused an increase in the number of contacts made between ligand binding residues and CGS-21680 in the mini-$G\alpha_s$ bound $A_{2A}R$ receptor but not in the antagonist-bound $A_{2A}R$. In accordance with this, important ligand binding residues, namely $M177^{5.38}$ $ASN253^{6.55}$ [59], also emerged on the allosteric pathway that links the ligand binding pocket to the intracellular domain of CGS-21680-bound $A_{2A}R$ in the presence of the linker. Therefore, these results suggest that the coupling between the ligand binding pocket and the intracellular domain of the receptor increased by the bivalent ligand. In accordance with that, volume of the ligand binding pocket was shrunk while the intracellular domain was expanded in agonist CGS-21680-bound $A_{2A}R$/mini-$G\alpha_s$. In spite of having no remarkable change at the ligand binding site, the volume of the intracellular domain was decreased in istradefylline-bound $A_{2A}R$. Importantly, modulation of the volume of the G protein binding site impacts contacts formed between intracellular domain and the effector as revealed by an increase in the respective energy term. Moreover, the decrease seen in the intracellular domain of antagonist-

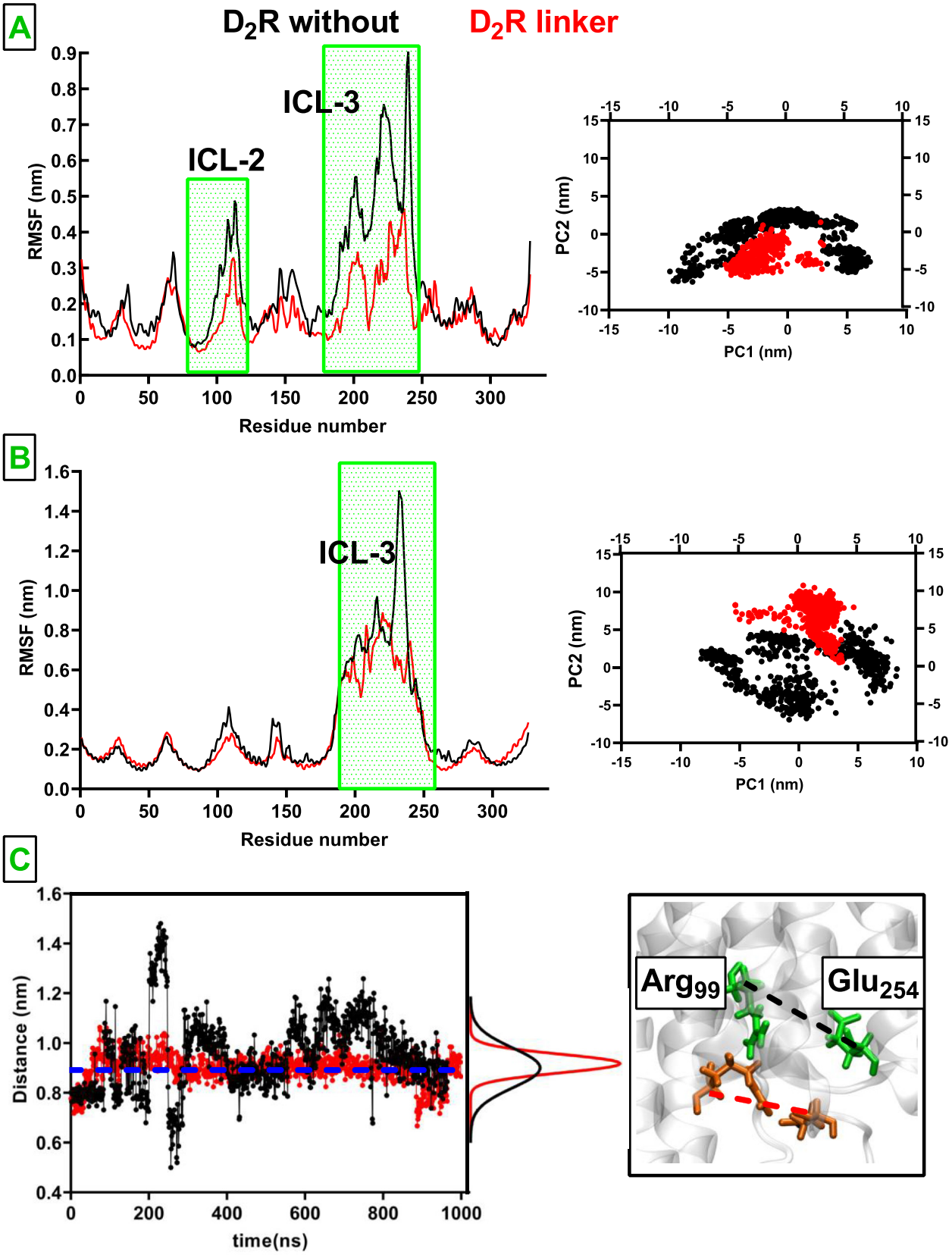

Fig. 9. Root mean square fluctuation (RMSF) and 2D principal component analysis (PCA) profiles pertaining to A. *apo* D_2R and **B**. agonist-bound D_2R/mini-$G\alpha_i$. The regions that showed difference between absence and presence of the linker are indicated with green rectangles. **C**. Time-line ionic lock distance sampled by *apo* D_2R in the presence (red) and absence (black) of the linker. The ionic lock distance measured in the crystal structure of eticlopride-bound D_2R (PDB ID:33PBL) is indicated with blue dash line. The RMSF and 2D-(PCA) plots of 2nd replicate is given in SI Fig. 5.

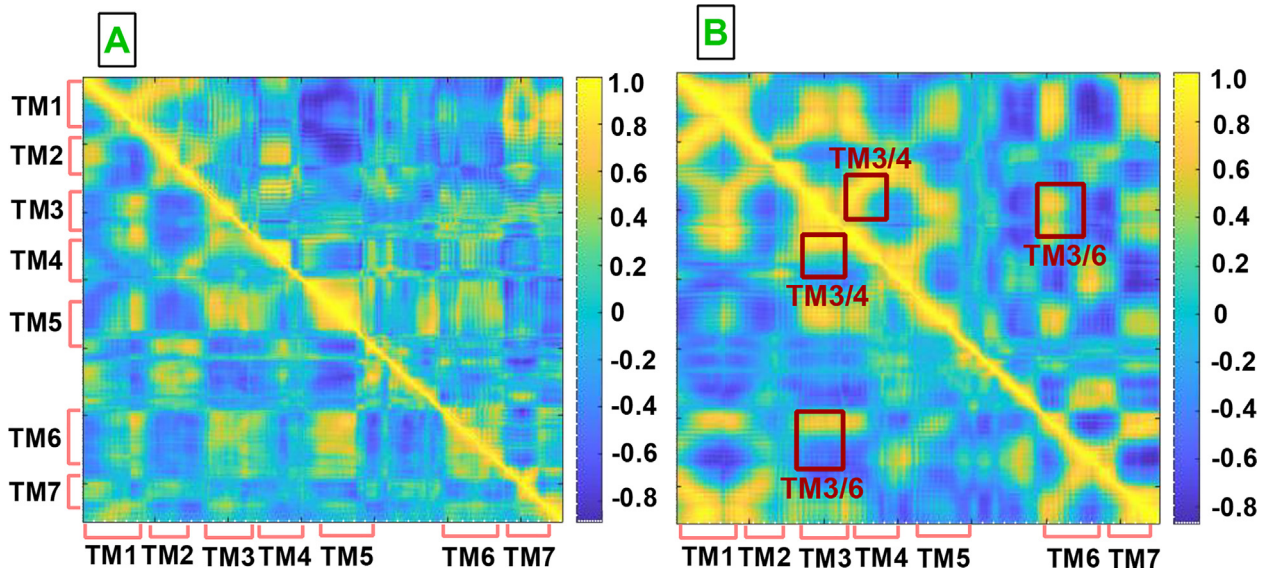

Fig. 10. Dynamic cross correlation maps (DCCM) are presented for **A**. agonist-bound D_2R/mini-Gα_i and **B**. *apo* D_2R. The upper diagonal in A and B correspond to DCCM of the system with linker whereas the lower diagonal correspond to those in the absence of linker. The DCCM plots are obtained by combining both replicas, and the DCCM plots of all the systems are given in SI Fig. 8.

bound $A_{2A}R$ might help prevent effector binding to the receptor. Herein, it is also important to emphasize that conformational preferences of some of the microswitches were modulated by the linker. Specifically, conserved Trp246$^{6.48}$ adopted side chain dihedral angles which provided residue 14 to be tightly packed against the sodium ion in antagonist-bound $A_{2A}R$. Also, another conserved residue, Tyr288$^{7.53}$, was oriented far from G protein binding site therein. On the other hand, no such alterations were observed in conformational preferences of these key residues in agonist-bound $A_{2A}R$ mini Gα_s. We also showed that above mentioned conformational changes led to alterations in residue correlation patterns and allosteric interaction network in the $A_{2A}R$ dimer. Specifically, we observed that conformational rearrangements which occurred during receptor activation were strengthened in the agonist-bound $A_{2A}R$-mini Gα_s by the presence of linker. Moreover, TM5 was emerged as the dominant participant of the allosteric interaction network in agonist-bound $A_{2A}R$-mini Gα_s in the presence of the linker. A similar trend was observed in $A_{2A}R$ upon complex formation with mini-Gs suggesting that impact of mini-Gs was accentuated by the presence of linker in CGS-21680-bound $A_{2A}R$. Besides $A_{2A}R$, the bivalent ligand also impacted *apo* D_2R in the neighboring D_2R dimer Notably, *apo* D_2R could sample wider range of ionic lock distances in the absence of the linker, whereas the distance was confined to the value which was sampled by the inactive receptor in the presence of the linker. In a study of Han et.al [23], it was shown that inverse agonist binding to one of the protomers in D_2R dimer enhanced D_2R signaling from agonist-bound D_2R. In addition, it has been also shown in a recent study that simultaneous binding of $A_{2A}R$ agonist/antagonist to $A_{2A}R$ dimer in $A_{2A}R/D_2R$ heterotetramer alleviated well-known antagonistic impact of $A_{2A}R$ on D_2R signaling. Since *apo* D_2R resembles inactive receptor in the D_2R dimer in the presence of the linker it is likely that the bivalent ligand decreases antagonistic impact of A_2R on D_2R signaling. From that perspective, the bivalent can be considered as a potential therapeutic molecule that can be used for treatment of Parkinson's disease, in which the efficacy of D_2R agonists is alleviated by antagonistic impact of $A_{2A}R$ [23]. The findings of this study can provide a methodology that can be followed to investigate impact of any bivalent ligand on a GPCR oligomer, thus paving a way for improving design strategies of such ligands and effective modulation of GPCR oligomers.

Author contributions

Samman Mansoor and Ozge Sensoy designed research, Samman Mansoor and Gulru Kayik performed research; Samman Mansoor analyzed data; Samman Mansoor and Ozge Sensoy wrote the paper; Serdar Durdagi and Gulru Kayik edited the paper.

Data and software availability

Classical and accelerated molecular dynamics simulation were performed using NAMD simulation package. Softwares used in the study are owned by their respective developers. The trajectories pertaining to both systems linker and without linker are deposited in OSF repository which can be assessed by the linkhttps://osf.io/tnpgz/?view_only=944246c89c06401d967628b52d71752b

Declaration of Competing Interest

The authors declare that they have no known competing financial interests or personal relationships that could have appeared to influence the work reported in this paper.

Acknowledgement

"The authors thank TUBITAK (reference number: 216S297) and COST Action CA15135, supported by COST (European Cooperation in Science and Technology) for providing funding. They also thank to TUBITAK ULAKBIM, High Performance and Grid Computing Center and Istanbul Medipol University for providing computational resources."

Appendix A. Supplementary data

Supplementary data associated with this article can be found, in the online version, athttps://doi.org/10.1016/j.csbj.2022.01.016.

References

[1] Bouvier M. Oligomerization of G-protein-coupled transmitter receptors. Nat Rev Neurosci 2001;2:274.
[2] Salahpour A, Angers S, Bouvier M. Functional significance of oligomerization of G-protein-coupled receptors. Trends Endocrinol Metab 2000;11:163–8.
[3] Jordan BA, Devi LA. G-protein-coupled receptor heterodimerization modulates receptor function. Nature 1999;399:697.
[4] Ilter M, Mansoor S, Sensoy O. Utilization of biased G protein-coupled receptor signaling towards development of safer and personalized therapeutics. Molecules 2019;24:2052.
[5] Bonaventura J, Navarro G, Casadó-Anguera V, Azdad K, Rea W, Moreno E, Brugarolas M, Mallol J, Canela EI, Lluús C, Cortés A. Allosteric interactions between agonists and antag- onists within the adenosine A2A receptor-dopamine D2 receptor heterotetramer. Proc Natl Acad Sci USA 2015;27:3609–18.
[6] Jenkins BG, Zhu A, Poutiainen P, Choi J-K, Kil K-E, Zhang Z, Kuruppu D, Aytan N, Dedeoglu A, Brownell A-L. Functional modulation of G-protein coupled receptors during Parkinson disease-like neurodegeneration. Neuropharmacology 2016;108:462–73.
[7] Riddy DM, Delerive P, Summers RJ, Sexton PM, Langmead CJ G. protein-coupled receptors targeting insulin resistance, obesity, and type 2 diabetes mellitus. Pharmacol Rev 2018;70:39–67.
[8] Arakaki AK, Pan W-A, Trejo J. GPCRs in cancer: protease-activated receptors, endocytic adaptors and signaling. Int J Mol Sci 2018;19:1886.
[9] Mansoor S, Kayik G, Alshahaby E, Guzel M, Durdagi S. O Sensoy. Development of novel therapeutic that can target multiple receptors for treatment of Parkinson's disease 2018;67.
[10] Ferré S. The GPCR heterotetramer: challenging classical pharmacology. Molecules 2015;36:145–52.
[11] Niethammer M, Tang CC, Ma Y, Mattis PJ, Ko JH, Dhawan V, Ei-delberg D. Parkinson's disease cognitive network correlates with caudate dopamine. Neuroimage 2013;78:204–9.
[12] Cotzias GC, Papavasiliou PS, Gellene R. Modification of Parkinsonism–chronic treatment with L-dopa. N Engl J Med 1969;280:337–45.
[13] LeWitt PA. Levodopa therapy for Parkinson's disease: pharmacokinetics and phar- macodynamics. Mov Disord 2015;30:64–72.
[14] Loonen AJ, Ivanova SA. New insights into the mechanism of drug-induced dyski- nesia. CNS Spectr 2013;18:15–20.
[15] Cieslak M, Komoszynski M, Wojtczak A. Adenosine A2A receptors in Parkinson's disease treatment. Purinergic Signal 2008;4:305.
[16] Lebon G, Edwards PC, Leslie AG, Tate CG. Molecular determinants of CGS21680 binding to the human adenosine A2A receptor. Mol Pharmacol 2015;87:907–15.
[17] Soriano A, Ventura R, Molero A, Hoen R, Casadó V, Cortés A, Fanelli F, Albericio F, Lluis C, Franco R, Royo M. Adenosine A2A receptor- antagonist/dopamine D2 receptor-agonist bivalent ligands as pharmacological tools to detect A2A–D2 receptor heteromers. J Med Chem 2009;52:5590–602.
[18] Stanton BZ, Chory EJ, Crabtree GR. Chemically induced proximity in biology and medicine. Science 2018:359.
[19] Xu Y, Duggineni S, Espitia S, Richman DD, An J, Huang Z. T.A synthetic bivalent ligand of CXCR4 inhibits HIV infection. Biochem Biophys Res Commun 2013;435:646–50.
[20] Krall N, Pretto F, Neri D. T.A bivalent small molecule-drug conjugate directed against carbonic anhydrase IX can elicit complete tumour regression in mice. Chem Sci 2014;24, 5:3640–4.
[21] Hübner H, Schellhorn T, Gienger M, Schaab C, Kaindl J, Leeb L, Clark T, Möller D, Gmeiner P. Structure-guided development of heterodimer-selective GPCR ligands. Nat Commun 2016;7:12298.
[22] Navarro G, Cordomíi A, Casadó-Anguera V, Moreno E, Cai N-S, Cortés A, Canela EI, Dessauer CW, Casadó V, Pardo L, Lluis C, Ferre S. Evidence for functional pre-coupled complexes of receptor heteromers and adenylyl cyclase. Nat Commun 2018;9:1–12.
[23] Han Y, Moreira IS, Urizar E, Weinstein H, Javitch JA. Allosteric communication between protomers of dopamine class A GPCR dimers modulates activation. Nat Chem Biol 2009;5:688.
[24] Carpenter B, Nehmé R, Warne T, Leslie AG, Tate CGT. Structure of the adenosine A2A receptor bound to an engineered G protein. Nature 2016;536:104–7.
[25] Liu W, Chun E, Thompson AA, Chubukov P, Xu F, Katritch V, Han GW, Roth CB, Heitman LH, IJzerman AP, Cherezov VST. Structural basis for allosteric regulation of GPCRs by sodium ions. Publ Am Assoc Adv Sci 2012;337:232–236..
[26] Friesner RA, Banks JL, Murphy RB, Halgren TA, Klicic JJ, Mainz DT, Repasky MP, Knoll EH, Shelley M, Perry JK, David E. Shaw, PF, Shenkin PST. Glide: a new approach for rapid, accurate docking and scoring. 1. Method and assessment of docking accuracy. J Med Chem; 2004:47;1739–1749..
[27] Halgren TA, Murphy RB, Friesner RA, Beard HS, Frye LL, Pollard WT, Banks JL. Glide: a new approach for rapid, accurate docking and scoring. 2. Enrich- ment factors in database screening. J Med Chem 2004;47:1750–9.
[28] Ballesteros JA, Weinstein H. Methods Neurosci 1995;25:366–428.
[29] Wang S, Che T, Levit A, Shoichet BK, Wacker D, Roth BL. Structure of the D2 dopamine receptor bound to the atypical antipsychotic drug risperidone. Nature 2018;555:269–73.
[30] Kang Y, Kuybeda O, de Waal PW, Mukherjee S, Van Eps N, Dutka P, Zhou XE, Bartesaghi A, Erramilli S, Morizumi T. Cryo-EM structure of human rhodopsin bound to an inhibitory G protein. Nature 2018;558:553–8.
[31] Robertson N, Rappas M, Doré AS, Brown J, Bottegoni G, Koglin M, Cansfield J, Jazayeri A, Cooke RM, Marshall FHT. Structure of the complement C5a receptor bound to the extra-helical antagonist NDT9513727. Nature 2018, 553, 111–114..
[32] Sastry GM, Adzhigirey M, Day T, Annabhimoju R, Sherman W. Protein and ligand preparation: parameters, protocols, and influence on virtual screening enrichments. Molecules 2013;27:221–34.
[33] Zhu K, Day T, Warshaviak D, Murrett C, Friesner R, Pearlman D. Antibody structure determination using a combination of homology modeling, energy-based refinement, and loop prediction. Proteins: Struct, Funct, Bioinf 2014;82:1646–55.
[34] Søndergaard CR, Olsson MH, Rostkowski M, Jensen JH. Improved treatment of ligands and coupling effects in empirical calculation and rationalization of pKa values. Molecules 2011;7:2284–95.
[35] Lomize AL, Pogozheva ID, Mosberg HI. Anisotropic solvent model of the lipid bilayer. 2. Energetics of insertion of small molecules, peptides, and proteins in mem- branes. J Chem Inf Model 2011;51:930–46.
[36] Lomize MA, Pogozheva ID, Joo H, Mosberg HI, Lomize AL. OPM database and PPM web server: resources for positioning of proteins in membranes. Nucl Acids Res 2011;40:370–6.
[37] Klauda JB, Venable RM, Freites JA, O'Connor JW, Tobias DJ, Mondragon-Ramirez C, Vorobyov I, MacKerell Jr AD, Pastor RW. Update of the CHARMM all-atom additive force field for lipids: validation on six lipid types. J Phys Chem B 2010;114:7830–43.
[38] Jo S, Kim T, Iyer VG, Im W. CHARMM-GUI: a web-based graphical user interface for CHARMM. J Comput Chem 2008;29:1859–65.
[39] Mark P, Nilsson L. Structure and dynamics of the TIP3P, SPC, and SPC/E water models at 298 K. J Phys Chem 2001;105:9954–60.
[40] Lee, J.; Cheng, X.; Swails, J.M.; Yeom, M.S.; Eastman, P.K.; Lemkul, J.A.; Wei, S.; Buckner, J.; Jeong, J.C.; Qi, Y.; Sunhwan Jo, V.S.P.; David A. Case, C.L.B.; Alexander D. MacKerell, J.B.K.; Im, W., T. CHARMM-GUI input generator for NAMD, GROMACS, AMBER, OpenMM, and CHARMM/OpenMM simulations using the CHARMM36 additive force field. J Chem Theory Comput 2015, 12, 405–413..
[41] Vanommeslaeghe, K.; Hatcher, E.; Acharya, C.; Kundu, S.; Zhong, S.; Shim, J.; Darian, E.; Guvench, O.; Lopes, V.I., P; Jr, M.A., T. CHARMM general force field: A force field for drug-like molecules compatible with the CHARMM all-atom additive biological force fields. J Comput Chem 2010, 31, 671–690..
[42] Phillips JC, Braun R, Wang W, Gumbart J, Tajkhorshid E, Villa E, Chipot C, Skeel RD, Kale L, Schulten K. Scalable molecular dynamics with NAMD. J Comput Chem 2005;26:1781–802.
[43] Evans DJ, Holian BL. The nose-hoover thermostat. J Chem Phys 1985;83:4069–74.
[44] Parrinello M, Rahman A. Polymorphic transitions in single crystals: A new molecular dynamics method. J Appl Phys 1981;52:7182–90.
[45] Miao Y, Nichols SE, Gasper PM, Metzger VT, McCammon T. Activation and dynamic network of the M2 muscarinic receptor. Proc Natl Acad Sci USA 2013;110:10982–7.
[46] Miao Y, Sinko W, Pierce L, Bucher D, Walker RC, McCammon JA. Improved reweighting of accelerated molecular dynamics simulations for free energy calculation. Chem Theory Comput 2014;10:2677–89.
[47] Tikhonova, I.G.; Selvam, B.; Ivetac, A.; Wereszczynski, J.; McCammon, J.A., T. Sim- ulations of biased agonists in the β2 adrenergic receptor with accelerated molecular dynamics. Biochemistry 2013, 52, 5593–5603..
[48] Miao Y, Nichols SE, McCammon JA. Free energy landscape of G-protein coupled receptors, explored by accelerated molecular dynamics. Phys Chem Chem Phys 2014;16:6398–406.
[49] Zhang F, Yuan Y, Li H, Shen L, Guo Y, Wen Z, Pu X. Using accelerated molecular dynamics simulation to shed light on the mechanism of activation/deactivation upon mutations for CCR5. RSC Adv 2018;8:37855–65.
[50] Kasahara K, Fukuda I, Nakamura H. A novel approach of dynamic cross correlation analysis on molecular dynamics simulations and its application to Ets1 dimer-DNA complex. PloS One 2014;9:e112419.
[51] Bhattacharyya M, Bhat CR, Vishveshwara S. An automated approach to network features of protein structure ensembles. Protein Sci 2013;22:1399–416.
[52] Oliveira SH, Ferraz FA, Honorato RV, Xavier-Neto J, Sobreira TJ, de Oliveira PS. KVFinder: steered identification of protein cavities as a PyMOL plugin. BMC Bioinf 2014;15:197.
[53] Yuan S, Filipek S, Palczewski K, Vogel H. Activation of G-protein-coupled receptors correlates with the formation of a continuous internal water pathway. Nat Commun 2014;5:1–10.
[54] Miao Y, McCammon JA. Mechanism of the G-protein mimetic nanobody binding to a muscarinic G-protein-coupled receptor. Proc Natl Acad Sci USA 2018;115:3036–41.
[55] Doré AS, Robertson N, Errey JC, Ng I, Hollenstein K, Tehan B, Hurrell E, Bennett K, Congreve M, Magnani F, Tate CG, Weir M, Marshall FH. Struc- ture of the adenosine A2A receptor in complex with ZM241385 and the xanthines XAC and caffeine. Structure 2011;19:1283–93.
[56] Xu F, Wu H, Katritch V, Han GW, Jacobson KA, Gao Z-G, Cherezov V, Stevens RC. Structure of an agonist-bound human A2A adenosine receptor. Publ Am Assoc Adv Sci 2011;332:322–7.

[57] McGraw C, Yang L, Levental I, Lyman E, Robinson AS. Membrane cholesterol depletion reduces downstream signaling activity of the adenosine A2A receptor. Biochim Biophys Acta, Biomembr 1861 2019:760–7.
[58] Kling RC, Clark T, Gmeiner P. T.U Comparative MD simulations indicate a dual role for Arg1323. 50 in dopamine-dependent D_2R activation. PloS One 2016;11:e0146612.
[59] Carpenter B, Lebon G. Human adenosine A2A receptor: molecular mechanism of ligand binding and activation. Front Pharmacol 2017;8:898.
[60] Dorfler M, Tschammer N, Hamperl K, Hubner H, Gmeiner P. Novel D3 selective dopaminergics incorporating enyne units as nonaromatic catechol bioisosteres: synthesis, bioactivity, and mutagenesis studies. J Med Chem 2008;51(21):6829–38.
[61] Tschammer, N., Elsner, J., Goetz, A., Ehrlich, K., Schuster, S., Ruberg, M., and Gmeiner, P. (2011). Highly potent 5-aminotetrahydropyrazolopyridines: Enantioselective dopamine D3 receptor binding, functional selectivity, and analysis of receptor- ligand interactions. J Med Chem 2011 54(7), 2477–2491..